EXPERIMENTAL VALIDATION OF CONTACT DYNAMICS SIMULATION OF CONSTRAINED ROBOTIC TASKS

J. Van Vliet and I. Sharf
Department of Mechanical Engineering
University of Victoria, British Columbia, Canada V8W 3P6
phone: (250) 721-6035, e-mail: isharf@uvic.ca

O. Ma
Macdonald Dettwiler Space and Advanced Robotics Limited
9445 Airport Road, Brampton, Ontario, Canada L6S 4J3
phone: (905)790-2800 ext.4535, e-mail: oma@spar.ca

ABSTRACT

Dynamics simulation plays a key role in the design, verification, and operation planning of the International Space Station manipulator systems because of the difficulties of ground-based physical tests with large flexible robotic systems. Modeling of contact dynamics has become essential to dynamics simulation of space station robotic operations (such as the assembly and maintenance of the station). To meet its mandate, the modeling and simulation tool must be of very high fidelity. This paper describes a research project aimed at experimentally validating a general contact dynamics simulation software developed by Macdonald Dettwiler Space & Advanced Robotics Ltd. (previously Spar Aerospace Ltd.). The experimental tests were carried out in the robotics laboratory at the University of Victoria. The validation results demonstrated that the software is capable of predicting realistic contact behavior during constrained robotic operations.

1. INTRODUCTION

Future applications of space manipulators will require execution of complex robotic operations involving constrained motions, such as Orbital Replaceable Unit (ORU) exchange and the assembly of the International Space Station. The contact objects may have complicated interface geometries, various physical properties, and arbitrary operational maneuvers. Ground-based physical testing of these operations with the entire robotic system will be extremely difficult. As a result, validated simulations become a prerequisite for the development of the corresponding control systems and the study of the operation missions.

Modeling contact dynamics is one of the most difficult aspects of developing a generic dynamics simulator for simulating robotic operations. Over the last few years, Macdonald Dettwiler Space & Advanced Robotics Limited (MDSAR) has developed a contact dynamics modeling and simulation tool as part of the Manipulator Development and Simulation Facility (MDSF). MDSF is a large software package developed by MDSAR for simulating general flexible multibody systems [1]. The package is currently employed for design, verification, operation planning, and engineering analysis of the International Space Station robotic systems: the Space Station Remote Manipulator System (SSRMS) and the Special Purpose Dexterous Manipulator (SPDM). Both robots are being built by MDSAR as a prime contractor to the Canadian Space Agency (CSA).

MDSF has undergone several validation exercises in the past and its simulation models of the SSRMS and SPDM have been accepted as truth models for the International Space Station Program. One previous validation of the MDSF's *contact dynamics* capability used the experimental results available in the literature [2]. Responses simulated by MDSF were compared with the peg-in-hole experiment where a cylindrical peg is slowly inserted in a hole with a milling machine. A detailed description of this validation has been reported in [3] where excellent agreement between MDSF and experiments is demonstrated.

In this paper, we report the results of a collaborative research project between University of Victoria and MDSAR on further experimental validations of MDSF's contact dynamics capability. This research was motivated by the need to expand the previous experimental validation to more complicated and diverse contact scenarios carried out with a robotic arm. The particular objectives of this research are stated below:

1. validate the contact dynamics methodology implemented in MDSF for robotic insertion of pegs of different geometries, materials and different insertion trajectories;
2. investigate the modeling effects of varying contact and manipulator parameters.

Proc. Fifth International Symposium on Artificial Intelligence, Robotics and Automation in Space, 1-3 June 1999 (ESA SP-440)

The experimental work to meet the objectives of the research has been conducted on the planar robotics facility at the University of Victoria [4]. The arm employed for the peg-insertion experiments has three degrees of freedom and is actuated by Harmonic Drive motors. An instrumented contact interface was added to the facility, as described in Section 2 of the paper. To simulate the peg insertion experiments, a model of the robotic arm, the actuators and contact interface was created in MDSF (see Section 3). In Section 4, we briefly discuss the validation of the manipulator model (arm and actuators) with unconstrained maneuvers under closed-loop and open-loop control. The key part of the paper, Section 5, contains experimental and simulation results for tasks with contact---the impact and peg insertion maneuvers. In the former, the peg is commanded to strike the side walls of the hole, thus allowing validation of the *impact* modeling capability of MDSF. A summary of all peg insertion experiments carried out with the test-bed is presented with results shown for a particular test-case. The plots illustrate the contact forces from simulation and experiment as well as the response of the arm. The paper concludes with comments on MDSF's overall capability and fidelity to simulate diverse contact scenarios for constrained robotic tasks.

2. EXPERIMENTAL TEST-BED

The experiments were conducted on the University of Victoria's robotics test facility which houses three robotic arms on a glass-topped table [4, 6]. The arm employed for the current work was configured with three Harmonic Drive actuators joined by aluminum square-section links. A contact dynamics interface was designed and consists of the special-purpose payload and an instrumented hole fixture. The payload, shown in Fig. 1, includes a Remote Center of Compliance device (RCC) that adds desired passive compliance about the peg tip. This compliance is necessary to facilitate the insertion operations without the involvement of a force control strategy. The end-effector is also instrumented with a planar force sensor to measure the forces and moment exerted on the peg. The range and bandwidth of the force sensor is ±222 N and 220 Hz. The peg, shown in Fig. 1 (also visible in Fig. 2), was designed to mimic the contact interface of RPCM which is one of the typical ORUs to be handled by SPDM.

The hole fixture, shown in Fig. 2, houses the 10 cm hole walls, hole force sensors and depth-of-insertion sensor. The hole is defined by two interchangeable hole profile pieces which are bolted to the inside faces of the load beams (flexures). Hole width is adjusted with spacers to enable insertions at different clearance ratios. On the outside faces, the load beams rest against compression load cells. Combined with the peg force sensor measurements, these allow determination of all contact forces when the peg is in contact with both sides of the hole (two-point contact). The depth of insertion sensor is a linear potentiometer which measures the deepest distance of any point on the peg. The sensor resolution is 0.1 mm in the measurement range of 100 mm.

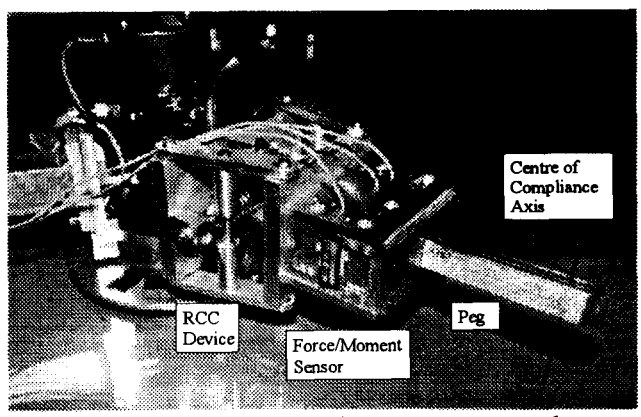

FIG. 1: Wrist joint, RCC, force/moment sensor, and peg

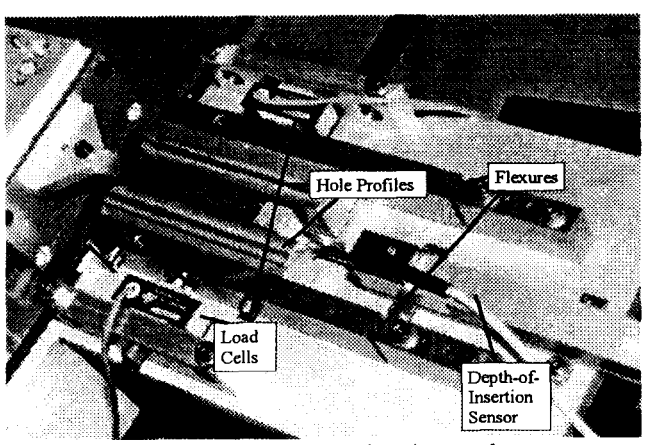

FIG. 2: Hole fixture assembly and an inserted peg

3. TEST-BED MODEL

To simulate the contact experiments with the facility described in Section 2, a model of the test-bed has been implemented in MDSF. As well, control code was developed to mimic the control module driving the physical test-bed. The MDSF model of the test-bed includes three major components: the robotic arm, the actuator dynamics and contact interface.

3.1 Arm model

The arm modeling involved defining the geometric, inertial and kinematic parameters for the component bodies of the robot. A schematic drawing of the arm subdivided into 22 component bodies is shown in Figure

3. It is noted that all component bodies were modeled as rigid with the exception of the rotational compliance of the RCC. Joint compliance was handled separately in the actuator dynamics code (see section 3.2).

The 22 component bodies were synthesized into five manipulator bodies, with two additional bodies describing the table and the hole fixture. These are shown in Figure 4 where we also annotated the articulations with *n-p*, where *n* is the body number and *p* is the node number. The articulation type is indicated by one of the following: a solid square (locked joint), empty circle (transient articulation joint), or solid circle (1-dof revolute joint).

3.2 Actuator Model

The actuator model was based on that in [5], combined with the results from joint identification experiments conducted in-house and manufacturer's specifications. Several experiments were carried out with individual joints to quantify the following actuator characteristics:

1. conversion from commanded rotor torque (in counts) to actual torque at the rotor;
2. startup (Coulomb) friction for gearbox;
3. load dependent Coulomb friction;
4. rate dependent (viscous) friction;
5. gearbox stiffness.

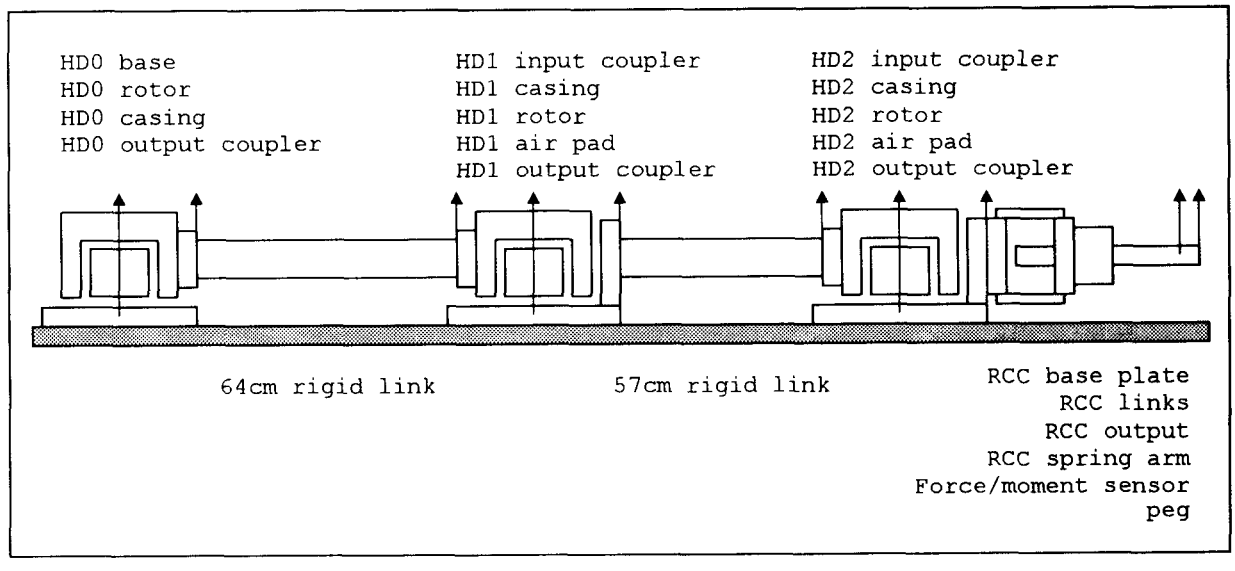

FIG. 3: Component bodies of the manipulator model

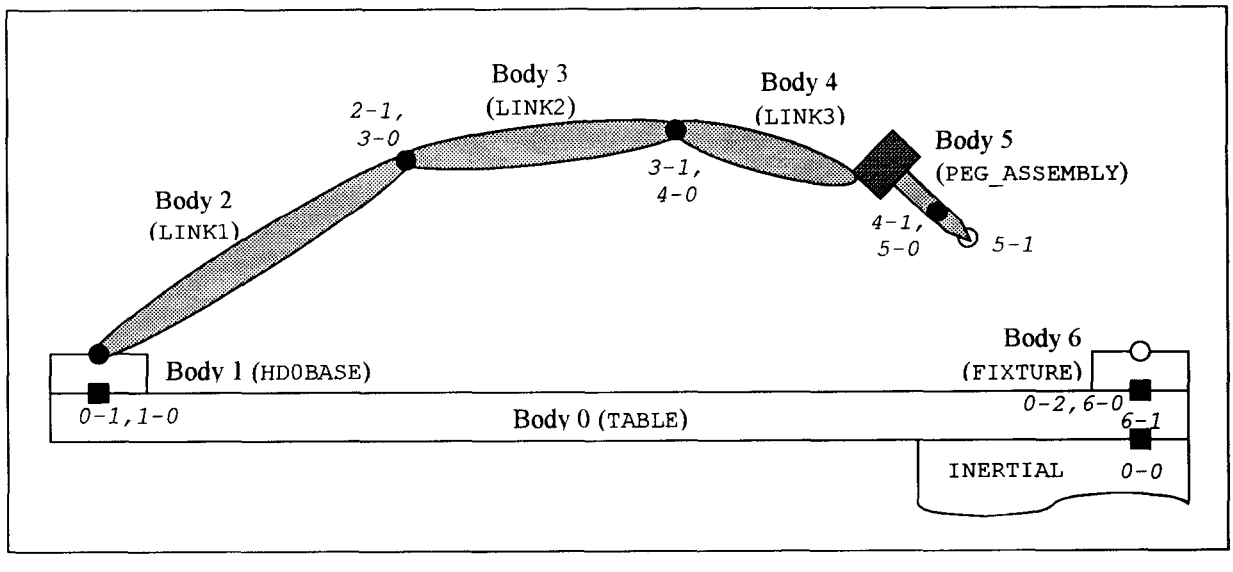

FIG. 4: Topology of the assembled manipulator model

The resulting actuator model includes the rotor inertia, gear ratio, gearbox flexibility, and friction. In accordance with manufacturer's specifications, the harmonic gearbox compliance is modeled as a three stage piece-wise linear spring with experimentally identified stiffness values. The static friction model employed here includes the load-dependent term, although it is nominally set to zero in the simulations conducted with MDSF. One unique aspect of the friction model is the *distributed* static friction in the gearbox. This was necessary to match the rotor angle vs. commanded torque curves observed when each joint was loaded and unloaded.

It is noted that due to the complexity of the identified actuator dynamics, the code implementing the actuator model was written separately and integrated with the rest of MDSF code, similarly to the control code.

3.3 Contact Model

The contact model created in MDSF defines the geometry of the contact bodies (peg and hole walls) as well as contact parameters. The latter represent the stiffness, friction, and damping properties of the contact surfaces. For our model, these were estimated or calculated as described below.

The contact stiffness is dominated by the compliance of the peg force sensor and the hole load cells since it is not included in the model of the manipulator system. The load cell stiffness values are directly available from manufacturer's specifications. These were used to estimate a range of the effective stiffness along the contact normal for peg inserted in the hole. For the majority of the simulations, the value of 0.91e6 N/m was used. This value was varied by an order of magnitude for MDSF sensitivity studies.

Peg insertion experiments with one-point sliding contact were performed to determine the coefficient of kinetic friction, μ_k, for aluminum and steel. The value of μ_k is employed by MDSF to evaluate the bristle friction model for contact friction [1]. The model also uses the coefficient of static friction which is set to 1.2 times the corresponding kinetic friction. It is widely acknowledged that friction depends on surface properties, such as roughness, cleanliness, and other factors, for example, speed of sliding, temperature and humidity. Special care was taken to ensure consistency of surfaces prior to conducting experiments. Under these conditions, the estimated values for steel and aluminum were: $\mu_{k,steel}$ = 0.22 and $\mu_{k,Al}$ = 0.65. As with contact stiffness, MDSF sensitivity simulations were conducted where μ_k was varied by ±20%.

Finally, the contact damping was set to 0.2 for all cases as this parameter was deemed less important for slow peg insertion maneuvers.

4. VALIDATION OF MANIPULATOR DYNAMICS MODEL

Prior to validating the contact dynamics model, it is necessary to validate the manipulator simulation model. To this end, a set of experiments and simulations was conducted with the manipulator moving free of contact. These constituted the *unconstrained* validation tests and allowed us to gain confidence in the modeling of the multibody arm, actuators, and control code. Two types of unconstrained experiments were conducted as follows.

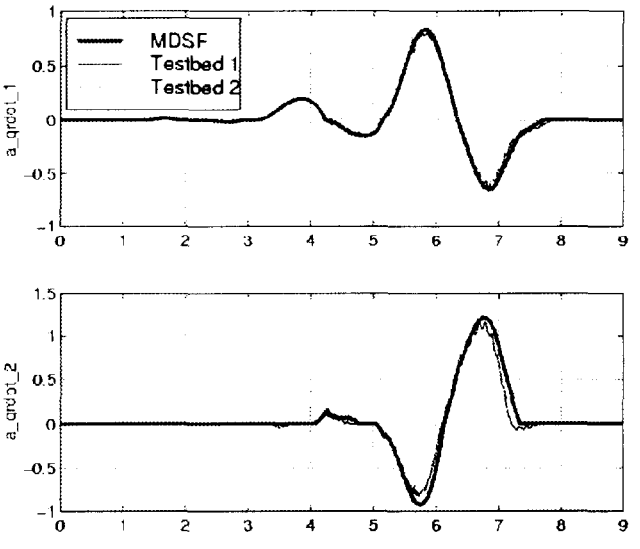

FIG. 5: Joint rates (rad/s) vs. time (sec) from unconstrained open-loop torque test

The first set of unconstrained maneuvers consisted of open-loop tests and was used to assess the accuracy of the inertial and friction elements of the MDSF model. The test involved commanding a smooth torque at a single joint, while other joints remained unactuated. The torque profile for each experiment included three cycles of increasing magnitude with the first peak typically below the static friction torque for the joint. Figure 5 presents the base and elbow joint rates obtained with the torque commanded at the base joint. The wrist is barely excited in this test-case and the corresponding results are not shown. The plots contain two sets of experimental results ('Testbed 1' and 'Testbed 2') and the simulated responses. As can be seen, the experimental curves show excellent repeatability and moreover, are in very good agreement with simulated profiles. There is a consistent pattern where the MDSF rates slightly overestimate the experimental rates. This is likely a result of unmodeled inertia in the system (such as signal and power cables

along the links), as well as small amount of friction between the joint air pads and the table.

In the second set of unconstrained maneuvers, closed-loop PD control is used to move the manipulator through the desired joint-level trajectory. In addition to providing further validation of the arm model, these tests act as a check on the control system implementation. The closed-loop experiments were conducted for a demanding fast maneuver with three sets of proportional feedback gains. Figure 6 displays the commanded torque and joint rate *error* for the elbow joint, obtained with the full gains. Note again the good agreement between the experimental and the simulated profiles. The visible disagreement between 5 and 6 seconds is immediately after a cusp in the desired joint rates. The agreement for the base joint has similar results, while that for the wrist joint is even better.

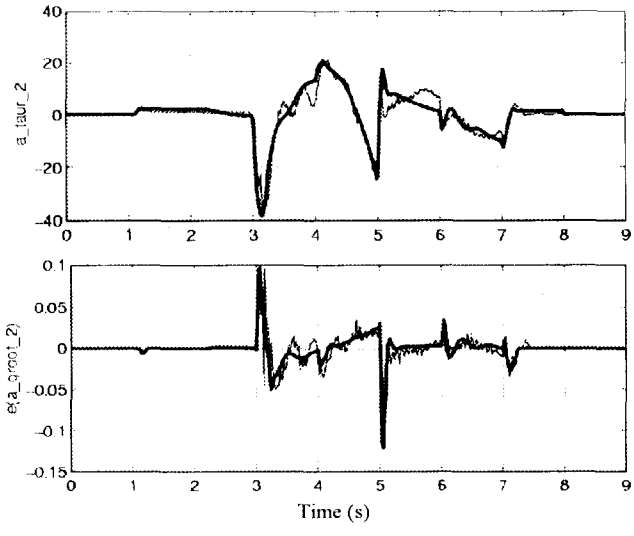

FIG. 6: Elbow joint torque (Nm) and rate error (rad/s) from unconstrained closed-loop torque test

For the unconstrained closed-loop maneuvers, there is little difference in the quality of the agreement between experiment and MDSF's predictions for different proportional gains. This is in contrast to constrained (contact) maneuvers where the agreement improves as proportional gains decrease to quarter of full gain values. This fact was attributed to the compliance in the links which is not modeled in MDSF, but becomes significant when manipulator arm is in contact with its environment (the hole fixture). Because the links are quite stiff, the effect of link flexibility is mitigated by lower joint stiffness caused by reducing the proportional gains of joint servos. This in turn leads to convergence of simulated and experimental results for constrained maneuvers.

5. VALIDATION OF CONTACT DYNAMICS

5.1 Impact Experiments

We begin the contact dynamics validation by presenting results for an impact maneuver where the peg strikes the sides of the hole. The desired Cartesian motion of the peg tip is shown in Figure 7. This maneuver, as well as the peg insertion experiments, is executed under PD joint control where the joint errors are generated from Cartesian motion errors. Since the facility is not instrumented with absolute end-effector position sensing, the 'actual' Cartesian motion is estimated from joint encoder measurements and forward kinematics.

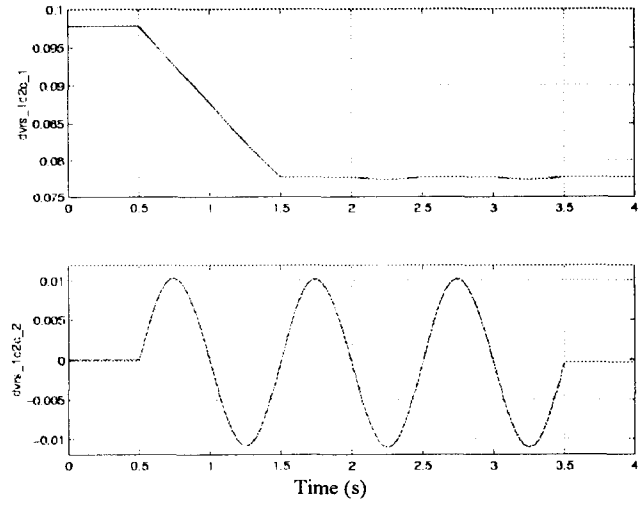

FIG. 7: Cartesian axial and lateral positions (m) of peg tip during impact test

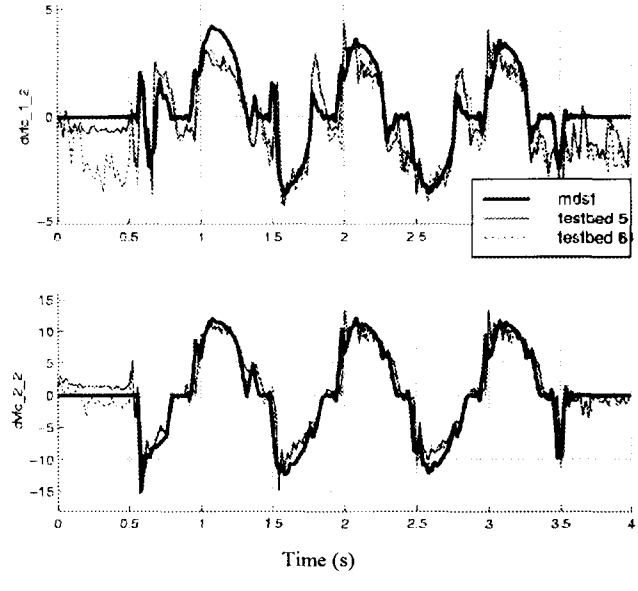

FIG. 8: Axial and lateral forces (N) of the impact test

As in the unconstrained experiments, the constrained tests were conducted with different proportional gains. We also note that all contact experiments were carried out under 'position' control described above, but without force control. It was deemed that the use of force control would mask the contact dynamics which was to be validated. On the other hand, without position feedback, as for instance in feedforward control, it would be difficult to ensure consistent peg insertions. Moreover, in such a situation, the contact dynamics would be contaminated by errors resulting from the inevitable inaccuracies in the dynamics model of the manipulator arm.

The axial and lateral forces on the peg are shown in Figure 8 for the impact test with the soft controller. Two sets of experimental results are presented ('Testbed 5' and 'Testbed 6') to illustrate the repeatability. As can be seen from Figure 8, the peg forces are in excellent agreement between experiment and simulation. The MDSF results are somewhat overdamped which indicates that a lower value for contact damping is more appropriate for the impact maneuver.

5.2 Peg Insertion Experiments

The full spectrum of the peg insertion experiments conducted in the scope of the present project covers the following scenarios:

1. three peg-hole configurations: steel peg-hole (one peg with chamfer and another without chamfer), aluminum peg-hole (one peg without chamfer);
2. three different hole widths;
3. four insertion trajectories distinguished by the initial lateral and angular misalignments of the peg with respect to the hole axis;
4. three different insertion speeds from quasi-static to relatively fast;
5. RCC active or locked where the Remote Center of Compliance was either active or inactive.

In addition, as before, experiments were conducted with different controller gains.

A typical peg insertion experiment consisted of three stages. The first involved moving the peg out of the hole from its home position flush against the right wall. At the end of this stage, the peg had the desired initial misalignments with respect to the hole. The next stage, which represents the beginning of the experiment, involved inserting the peg into the hole, at constant speed. Most experiments were executed at 1 cm/sec insertion speed and this stage took 10 seconds. After a 1 second hold at the end of the insertion, a removal stage was initiated to withdraw the peg from the hole. At the end of the experiment (typically 21 seconds), the arm is relaxed by commanding zero joint torques.

With the parameter variations listed above, we were able to produce a range of contact situations from one-point contact insertion and removal, to two-point contact occurring during insertion and removal, to peg jamming. At the inception of jams, the contact forces increase rapidly which often resulted in load cell overload condition and premature termination of the experiment. In the following, we present results for a insertion and removal maneuver and a jamming situation.

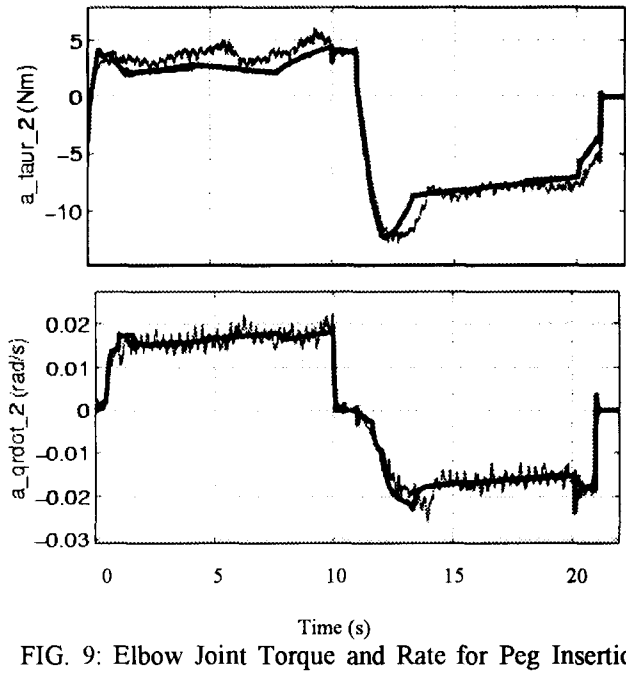

FIG. 9: Elbow Joint Torque and Rate for Peg Insertion Test (RCC active)

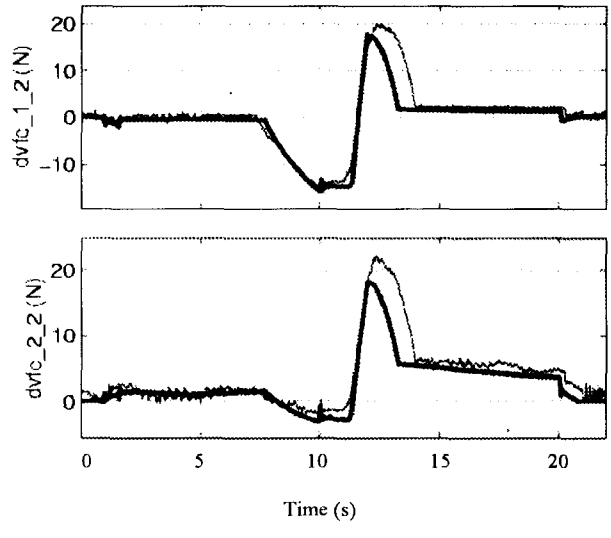

FIG. 10: Axial and lateral forces applied to peg tip during peg insertion (RCC active)

In the peg insertion test considered here, a square steel peg, 12.45mm (0.49") wide, is inserted at 10 mm/sec into a hole of 15.49mm (0.61") wide. The initial misalignment of the peg is nominally a -5 mm lateral offset and 0.12 rad peg angle. The same experiment was conducted with RCC active or inactive, the latter resulting in a jamming situation. Figure 9 shows the commanded joint torque and joint rate response for the elbow joint, while Figure 10 shows the forces on the peg, with RCC active. In this insertion experiment, the peg makes a transition from one-point contact to two-point contact at 7.3 seconds during the insertion stage, and the reverse happens at 14.0 seconds during the removal. The results illustrate very good agreement between simulation and experiment. The somewhat significant discrepancy is observed during the two-point contact stage of the removal (11-14 seconds). This is typical of many test-cases investigated experimentally and in simulation. Our parameter sensitivity studies also indicate that the two-point contact phase is particularly affected by contact stiffness and friction values.

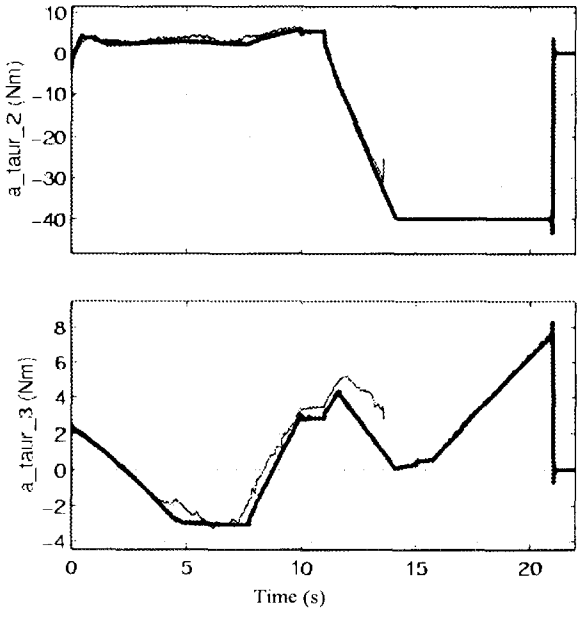

FIG. 11: Elbow and wrist joint torques for peg insertion test (RCC inactive)

The results for the jamming case with RCC inactive are shown in Figure 11, which displays the commanded elbow and wrist torques and Figure 12, exhibiting axial and lateral forces on the peg, as well as the depth of insertion. In this case, the experiment was terminated prematurely (at about 13.3 seconds) because of the aforementioned overload protection measure, which in turn indicates the inception of a jam. The simulation results clearly predict a jamming condition as the peg remains stuck until the nominal end of the maneuver (21 seconds). As can be seen from Fig.12, up until the experiment was terminated, the agreement between the experimental data and simulation results for both tip position and contact forces is very good.

As noted earlier, many peg insertion experiments and simulations with various different conditions have been carried out in this investigation. In addition to demonstrating very good quantitative agreement, our results led to a number of intuitive qualitative observations which hold true for both experiment and MDSF simulation:

(1) jamming situations are more likely to occur with a stiffer arm (such as with locked RCC);
(2) occurrence of jams increases when the clearance between the peg and hole decreases or the misalignment between the peg and hole increases.
(3) jams are more probable during the removal operation, and in fact, at the initiation of a removal;
(4) for a particular insertion/removal maneuver, removal forces tend to be larger than insertion forces;
(5) results during two-point contact are much more sensitive to contact stiffness and friction than during one-point contact. As a consequence, similar observations hold for jams.

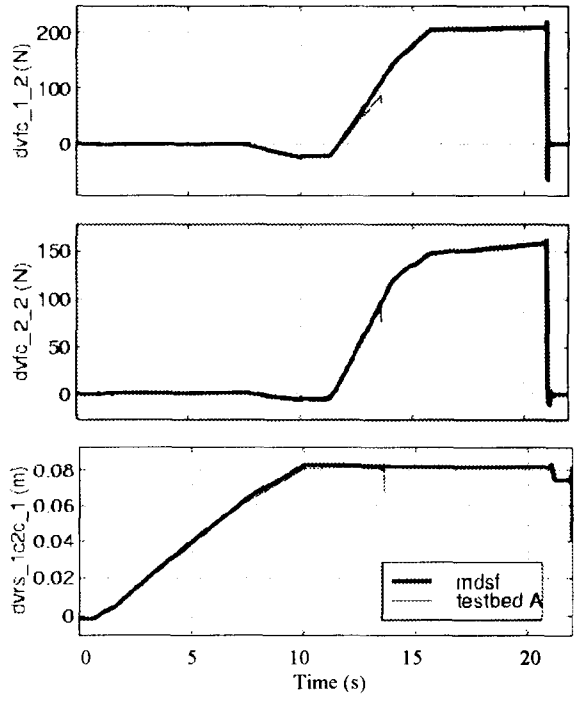

FIG. 12: Top two plots: axial and lateral forces applied to peg tip. Bottom plot: depth of insertion of the peg tip during peg insertion (RCC inactive). The test data ends at about 13.3 s.

6. CONCLUSIONS

In this paper, we presented a selection of the results from the research project on the experimental validation of the general contact dynamics modeling and simulation software developed by Macdonald Dettwiler Space and Advanced Ltd. The venue for the experiments was the University of Victoria robotics facility retrofitted with a specially designed peg-and-hole interface. A model of the manipulator arm was created in MDSF and validated before integrating it with the contact dynamics model. The simulation model was then employed to simulate the experiments conducted with the facility. In general, the agreement between simulation results and experiments is very good. This holds true for a variety of contact geometries, materials, and insertion speeds investigated as part of the objectives of the project. Based on the results of the parameter sensitivity studies conducted with MDSF simulation, we conclude that the quantitative agreement between simulations and experiments could be further improved by tuning parameters of the contact dynamics model and adding manipulator link compliance to the arm dynamics model.

Acknowledgements

Funding support from the National Science and Engineering Research Council (NSERC) and Canadian Space Agency (CSA), through research grant #210114, is acknowledged. Funding and technical support from Macdonald Dettwiler Space & Advanced Limited is also acknowledged.

References

[1] Ma, O., Buhariwala, K., Roger, N., MacLean, J. & R. Carr, (1997). "MDSF---A Generic Development and Simulation Facility for Flexible, Complex Robotic Systems," *Robotica*, Vol. 15, pp. 49-62.

[2] Whitney, D.E., (1982). "Quasi-Static Assembly of Compliantly Supported Rigid Parts," *Journal of Dynamic Systems, Measurement, and Control*, Vol. 104, pp. 65-77.

[3] Ma, O., (1995). "Validation of MDSF Contact Dynamics Simulation against Whitney's Analytical & Experimental Results", *Spar Technical Report* CSS-TN.206.

[4] Nahon, M., Damaren, C., Goncalves, J. and A. Bergen, [1995]. "Test Facility for Multi-Armed Space-Based Manipulators," *Canadian Aeronautics and Space Journal*, Vol. 41, No. 4, pp. 150-162.

[5] Bridges, N.M. & D.M. Dawson, [1993]. "Redesign of Robust Controller for RLFJ Robotic Manipulators Actuated with Harmonic Drives," *Proc. American Control Conference*, San Francisco, pp. 2507-2510.

[6] Van Vliet, J., and I. Sharf, [1998]. "Development of a Planar Macro-Micro Manipulator Facility: From Design through Model Validation," *Canadian Aero. and Space Journal*, Vol. 44, pp. 40-50.